Formation Mechanisms of Nanostructures by Nanosecond Laser Ablation of Multi-component Amorphous Alloys in Water

S. Yaginuma*[1], R. Ninomiya[2], D. V. Louzguine-Luzgin[3], K. Oshida[4], X. Fang[5], K. Ishikawa[2], and Y. Miyajima[2]

[1]*National Institute of Technology (KOSEN), Nagano College, Japan*
[2]*Graduate School of Natural Science and Technology, Kanazawa University, Japan*
[3]*Advanced Institute for Materials Research (WPI-AIMR), Tohoku University, Japan*
[4]*Institute for Aqua Regeneration, Shinshu University, Japan*
[5]*School of Electronics and Computer Science, University of Southampton, UK*
**Corresponding author's e-mail:* s_yaginuma@nagano-nct.ac.jp

We report on the nanosecond pulsed laser ablation of quaternary Pd-based and Zr-based amorphous alloy targets in water. Our comparative measurements and analyses of the size, shape, structure, and composition of laser ablation products reveal the formation of nanoparticles and nanowires with partially or fully amorphous states. The formation mechanisms of the amorphous alloy nanowires are discussed in terms of material properties (fiber spinnability, glass-forming ability, and oxidation resistance), which are different from the conventional explanations of interconnection between nanoparticles and linear growth from nanocluster level.

DOI: 10.2961/ilmn.2025.02.2010
Keywords: quaternary alloy, amorphous, nanowire, nanoparticle, pulsed laser ablation in liquid, nanosecond laser

1. Introduction

The physical and chemical properties of low-dimensional nanostructures such as nanoparticles and nanowires can be controlled by their size and shape [1-3]. Nanostructures of multi-component alloys have attracted growing interest in various fields including nano-devices, energy technologies, catalysis, and biomedicine, due to their ability to combine the effects of nanoscale size and shape with the freedom of choosing alloy composition and process design [4-7]. Amorphous alloy nanowires are expected to exhibit unique one-dimensional (1D) functionalities based on their excellent mechanical properties (high strength and toughness, corrosion and wear resistance) and thermoplasticity [5,8,9]. The fabrication of such amorphous alloy nanostructures requires a non-equilibrium process to rapidly solidify nano-sized molten alloys, for which fabrication methods such as nanoimprinting [5], co-sputtering [8], and gas atomization [9] have been developed recently. In particular, the gas atomization provides the mass production of amorphous alloy droplets and wires. For quaternary Pd-based alloys, the conditions were optimized for atomized wires to become the main product [10]. However, it remains difficult to reduce the diameter and its distribution (particles: 0.5–20 μm, wires: 50 nm–2 μm) and to stably disperse the products in a solvent.

Pulsed laser ablation in liquid (PLAL), known as a green (environmentally friendly) method, has been developed to synthesize pure metal crystalline nanoparticles with diameters as small as 10 nm [11,12]. These nanoparticles are formed by Rayleigh–Taylor (RT) instability [13]. That is, the RT instability occurs when a dense molten layer of target material is rapidly accelerated by a surrounding lighter liquid, leading to the sudden ejection of molten nano- to submicron-scale droplets, which then rapidly cool and solidify in the liquid. Since these thermal and hydrodynamic effects are more pronounced on nanosecond (ns) time scales, ns-PLAL should be suitable for the purpose of synthesizing and dispersing amorphous alloy nanostructures in liquids. Nevertheless, there are few reported cases of its application to multi-component amorphous alloys [6,14].

Here, we study the generation of low-dimensional nanostructures by ns-PLAL of quaternary Pd-based and Zr-based amorphous alloy targets. In common with both the targets, particles with a broad size distribution ranging from microscale to nanoscale are synthesized as the main product and dispersed in water. In the case of the Zr-based alloy target, a small number of 1D nanowires are shown to coexist. Furthermore, partially or fully amorphous states are found in respective nanostructures of both particles and wires. In order to increase the ratio of nanowires to nanoparticles, we discuss the formation mechanisms of the amorphous alloy nanostructures and propose that spinnability (defined as an ability to form into threads or fibers [15]) is a possible main mechanism for forming the observed nanowires.

2. Methods

Among multi-component alloys, $Pd_{42.5}Cu_{30}Ni_{7.5}P_{20}$ [16] and $Zr_{70}Cu_{15}Al_{10}Fe_5$ [17] were selected as target materials. These alloys with an amorphous nature were fabricated using arc melting and casting equipment. Each alloy target with a disk shape was submerged in water medium at room temperature, and its surface was irradiated with focused fundamental beams (wavelength of 1064 nm) of a nanosecond pulse-width laser (repetition rate of 10 Hz). The details of the fabrication process using a Nd:YAG laser (Litron Lasers Nano SG 150) were described elsewhere [18,19].

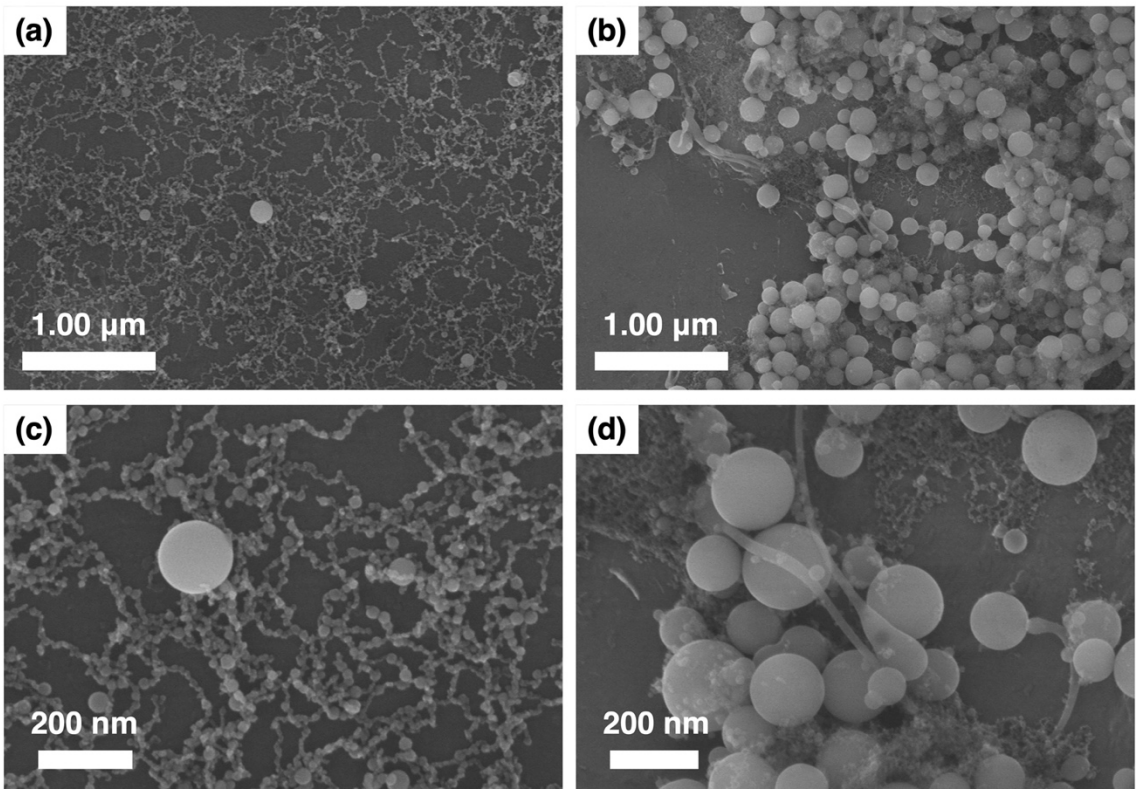

Fig. 1 SEM images of the products formed by laser ablation of the $Pd_{42.5}Cu_{30}Ni_{7.5}P_{20}$ (a and c) and $Zr_{70}Cu_{15}Al_{10}Fe_5$ (b and d) targets in water. The (c) and (d) images magnify the central part of the (a) and (b) images, respectively. The laser irradiation energy was 50 mJ/pulse. The products were supported on aluminum foil for imaging.

The products of laser ablation of multi-alloy targets were dispersed in the water as a common feature.

Structural and compositional characterizations were performed with scanning electron microscopy (SEM), transmission electron microscopy (TEM), and energy dispersive X-ray spectroscopy (EDXS). Shared facilities were used: SEM (Hitachi High-Tech SU8000 working at 15 kV), TEM (JEOL JEM-ARM200F NEOARM at 200 kV and JEM-2100F at 80 kV), and EDXS (JEOL JED-2300T). Samples with laser ablation products dispersed in water were dropped from the same lot onto an Al foil for SEM observation and onto a Mo microgrid for TEM observation, respectively, and were allowed to dry naturally.

3. Results

To grasp the overall size and shape information of the two types of products (due to differences in alloy composition) and to confirm their reproducibility, we compare SEM images at the same magnification. Figures 1(a) and 1(c) show the SEM images obtained from the products of the $Pd_{42.5}Cu_{30}Ni_{7.5}P_{20}$ target, and Fig. 1(c) is a high-resolution image of Fig. 1(a). Fig. 1(a) indicates wire-like features at first glance; however, Fig. 1(c) reveals that they are interconnected nanoparticles. For the Pd-based alloy target, nanoparticles are thus the main products, and nanowires can hardly be recognized. During the drying process, some of the smaller nanoparticles may adhere to each other to form wire-like features, while other nanoparticles may adhere to the surface of exposed large particles.

Figures 1(b) and 1(d) show the exemplary and high-magnification SEM images obtained from the products of the $Zr_{70}Cu_{15}Al_{10}Fe_5$ target, respectively. Submicron particles are observed along with some aggregates. It should be noticed that a small number of nanowires coexist, as shown in Fig. 1(d). The nanowires have an elongated shape which is clearly different from the wire-like features observed in Fig. 1(c). In addition, Fig. 1(d) suggests that the agglomerates are composed of fine nanoparticles adhered to the exposed substrate during the drying process.

TEM observations allow us to clarify the atomic-level structure and morphology of the ablation products. Figs. 2(a) and 2(b) reproduce the results of SEM observations in Figs. 1(c) and 1(d), respectively. In common with the Pd-based alloy and the Zr-based alloy targets, nanoparticles were obtained as the main product, dispersed in water. As a difference, only nanoparticles were observed in the case of Pd-based alloy target, whereas nanowires were also formed in the case of Zr-based alloy target. In comparison of different laser irradiation energies (20 to 80 mJ/pulse), the nanoparticle formation efficiency increased with increasing energy, but there was no significant change in the average particle diameter of several tens of nanometer. For the ns-PLAL of the Pd-based and Zr-based alloy targets, the formation mechanism of these nano- to submicron-scale particles would be consistent with an understanding based on RT instability, from the pure metal analogy [13]. We also suppose some of the smaller nanoparticles to be driven by secondary instabilities, which will be discussed later in this paper.

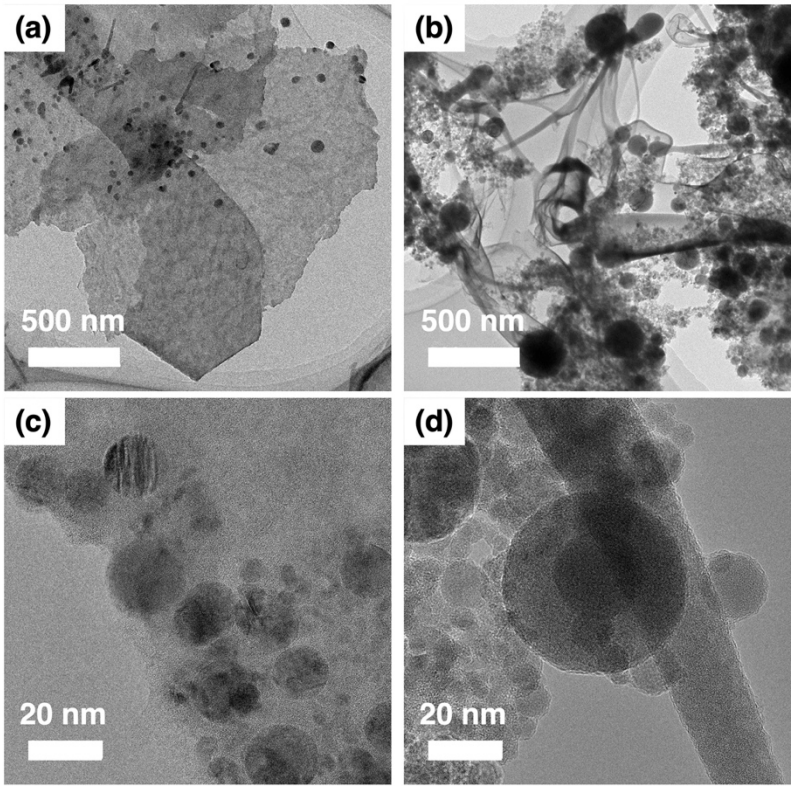

Fig. 2 Bright-field (a and b) and high-resolution (c and d) TEM images of the products formed by laser ablation of the $Pd_{42.5}Cu_{30}Ni_{7.5}P_{20}$ (a and c) and $Zr_{70}Cu_{15}Al_{10}Fe_5$ (b and d) targets in water. The laser irradiation energy was 80 mJ/pulse.

Figure 2(c) shows a TEM image of nanoparticles among the products of the $Pd_{42.5}Cu_{30}Ni_{7.5}P_{20}$ target. Crystalline and amorphous states vary from particle to particle or are mixed within a single particle. On the other hand, in the case of the $Zr_{70}Cu_{15}Al_{10}Fe_5$ target, the formation of nanowires is reconfirmed (Fig. 2(d)). Furthermore, Fig. 2(d) indicates nanoparticle and nanowire formation with partially or fully amorphous states. The observation of partially amorphous nanoparticles was previously reported [6,14].

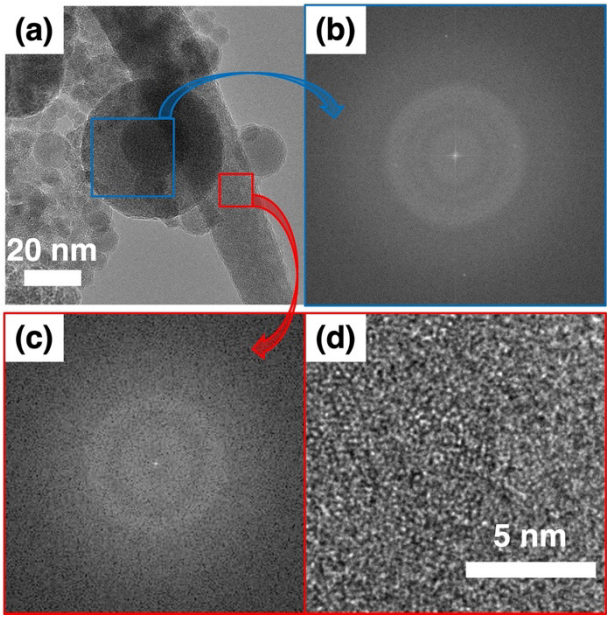

Fig. 3 (a) Identical TEM image to Fig. 2(d). Fast Fourier transform (FFT) of a nanoparticle (b) and a nanowire (c), indicated by blue and red squares in (a), respectively. (d) Magnified view of the area of the red square, corresponding to FFT (c).

To gain deeper insight into the observed amorphous and crystalline structures of the products formed by laser ablation of $Zr_{70}Cu_{15}Al_{10}Fe_5$ target, we closely examined TEM image in Fig. 3(a) and performed first Fourier transform (FFT) analysis of a nanoparticle and a nanowire taken from the area of blue and red squares, respectively. As can be seen from Fig. 3(b), not only amorphous halo but also crystalline spots are observed, indicating the coexistence of partially amorphous and crystalline structures within a single particle [also see Fig. 2(d)]. On the other hand, Fig. 3(c) shows a characteristic halo ring pattern, indicating the amorphous structure of the nanowire. Disordered atomic configurations in Fig. 3(d) further confirms that the formed nanowire is amorphous.

TEM-EDXS elemental mapping visualizes the distribution of alloy composition and the effect of oxidation. Figs. 4(a) and 4(b) show the constituent elements and oxygen maps taken from nanoparticles generated by the laser ablation of the $Pd_{42.5}Cu_{30}Ni_{7.5}P_{20}$ and $Zr_{70}Cu_{15}Al_{10}Fe_5$ targets, respectively. In Fig. 4(a), the selected peaks in the EDXS spectrum for these maps are Pd *K*, Cu *K*, Ni *K*, P *K*, and O *K*. It has been demonstrated that PLAL can preserve the composition ratios of alloy targets to synthesize nanoparti-

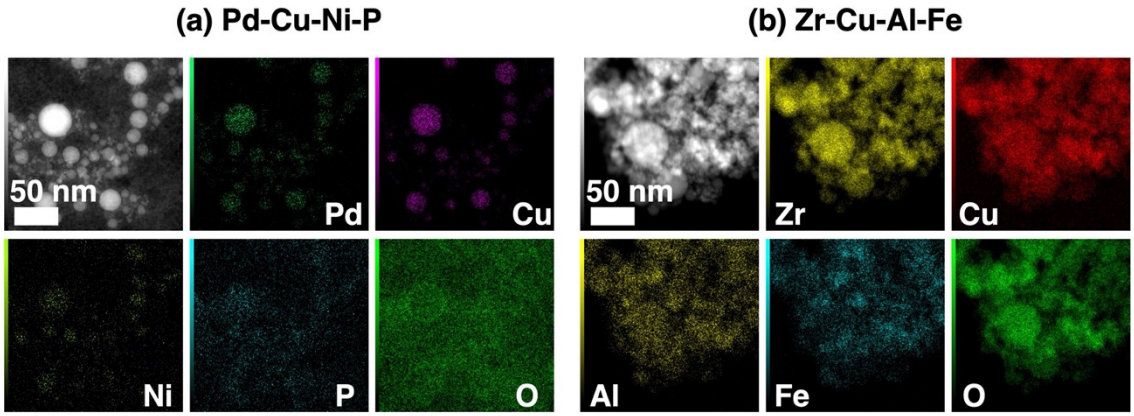

Fig. 4 Bright-field TEM image (upper left) as well as corresponding EDXS elemental mapping images (as marked) of the nanoparticles formed by laser ablation of the $Pd_{42.5}Cu_{30}Ni_{7.5}P_{20}$ (a) and $Zr_{70}Cu_{15}Al_{10}Fe_5$ (b) targets in water.

cles with the same composition [6,14], however, P tend to be at lower concentrations, compared with the concentrations of Pd, Cu, and Ni. While Pd, Cu, and Ni have very similar distributions per particle, O, which is not a constituent element, has a nearly uniform distribution on the map, indicating little oxidization effect on the nanoparticles or only surface oxidization. In Fig. 4(b), the peaks Zr *L*, Cu *K*, Al *K*, Fe *K*, and O *K* are selected. For Fe, some particles with lower concentrations are observed. Except for Fe, all the elements, including O, have very similar distributions per particle, suggesting that the synthesized particles are oxidized.

4. Discussion

We now discuss the formation mechanism of the observed Zr-based alloy nanowires in Figs. 1(d) and 2(d). In general, formation mechanisms of 1D nanowires by PLAL can be categorized into (1) interconnection between nanoparticles and (2) linear growth of nanoclusters [20]. The strong evidence for the former fusion mechanism was the morphology of silver nanowires, as their diameter was comparable to as-prepared nanoparticles and the shape of spherical nodules was similar to the original nanoparticles [21]. However, as can be seen from Figs. 1(d) and 2(d), the diameter of the Zr-based alloy nanowires does not seem to correlate directly with the diameter of the nanoparticles, and there are no nodules derived from the nanoparticles. The TEM images in the paper reporting gold chain formation [22] look rather like Fig. 1(c). Therefore, the formation mechanism of the observed Zr-based alloy nanowires is unlikely to be explained by the (1) interconnection between nanoparticles. As for (2) linear growth, although various interpretations have been proposed, their main mechanism is nuclear growth from the nanocluster level, such as vapor–liquid–solid-like growth [23], and reliable explanations are still lacking for some materials. RT instability is known to influence the dynamics of the ablation plume or the collapse of cavitation bubbles during ns-PLAL and thus nanoparticle formation [13], but is insufficient to explain the nanowire formation.

We propose spinnability as a possible mechanism for the formation of amorphous alloy nanowires by ns-PLAL. The spinnability is defined as an ability to form into threads or fibers [15]. As a consequence of RT instability, molten filaments or jets may form (which leads to a sudden ejection of molten droplets). Once these long and narrow liquid-phase structures are formed, surface tension causes them to break up into nanoparticles, minimizing their surface area. This process is called capillary instability or Rayleigh–Plateau (RP) instability and can be secondary to RT instability, as illustrated in Fig. 5(a). For the RP instability, $d = 1.88\ D$ is derived, where D is diameter of the liquid cylinder/thread, d is diameter of the droplet formed by the breakup of the thread (and λ is the wavelength of the fastest growing mode). The scenario of RT-induced jetting followed by RP breakup is consistent with recent modeling and theoretical studies [24]. However, when the viscosity of these molten filaments is high, they are stretched into nanowires (Fig. 5(b)). This spinnability is the defining feature enabling the formation of amorphous alloy nanowires under gas atomization [9,10]. The present ns-PLAL is analogous to gas atomization in that the material is evaporated and cooled (by solvent molecules) instantaneously, and we believe that the spinnability is the main mechanism of the observed nanowire formation in ns-PLAL as well.

In ns-PLALs of pure metals, the main products are generally crystalline nanoparticles. One of the reasons why the size, shape (dimensionality) and structure of the ns-PLAL products of the quaternary alloys discussed here differ from those of pure metals is due to their high glass-forming ability (GFA) inherent to the alloy composition. In this respect, the alloy composition of $Pd_{42.5}Cu_{30}Ni_{7.5}P_{20}$ is known to have the highest GFA and oxidation resistance among metallic glasses [10,16]. GFA is the capacity of a material to avoid crystallization during cooling and instead form an amorphous solid or a glass with low viscosity in the supercooled liquid region. Therefore, Pd-based alloys with high GFA should be promising candidates for both amorphization and wire formation. However, the ns-PLAL of the $Pd_{42.5}Cu_{30}Ni_{7.5}P_{20}$ target didn't yield the expected products, *i.e.*, amorphous nanowires. Possible reasons for this include the laser parameter of nanosecond pulse width. This causes the nanostructures to be trapped in cavitation bubbles, resulting in insufficient cooling rates [6,14]. However, if this

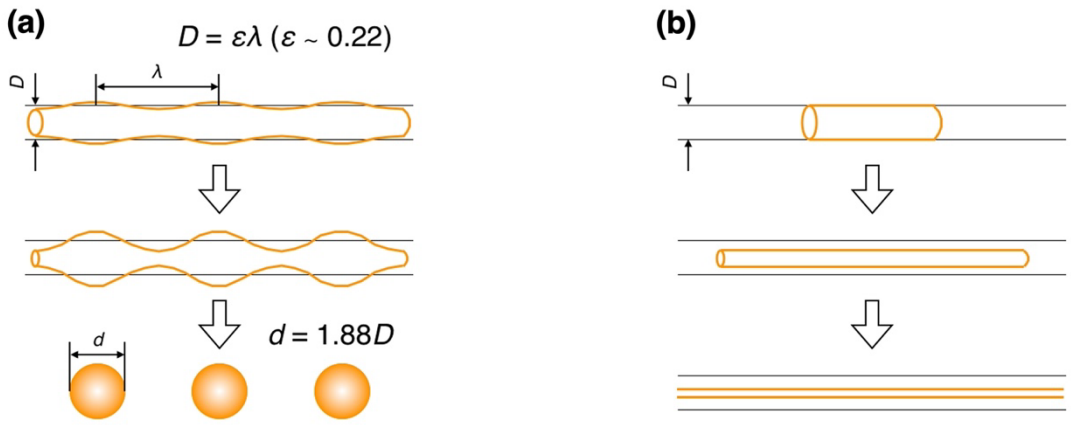

Fig. 5 Schematic illustration of (a) capillary instability (Rayleigh-Plateau instability) and (b) spinnability, which result in the droplet and wire formations of viscous ligaments, respectively.

reason is true, an additional question arises as to what factors could have contributed to demonstrate the amorphization and wire formation in the alloy composition of $Zr_{70}Cu_{15}Al_{10}Fe_5$, which has a lower GFA than $Pd_{42.5}Cu_{30}Ni_{7.5}P_{20}$. TEM-EDXS elemental mapping reveals the oxidation of the ns-PLAL products [Fig. 4(b)], which is consistent with $Zr_{70}Cu_{15}Al_{10}Fe_5$ has lower oxidation resistance than $Pd_{42.5}Cu_{30}Ni_{7.5}P_{20}$. Indeed, metal oxides more readily vitrify [6] and form wires [20]. Oxides tend to have a high melt viscosity under rapid cooling conditions [9,25], which strongly manifests their spinnability. The nanofiber fabrication by laser ablation of silica (SiO_2) glass was reported and similar mechanism to favor the formation of nanowires/nanofibers was discussed (although the term "spinnability" did not appear) in Ref. [26].

5. Summary

We have selected Pd-based and Zr-based alloy targets from among multi-component alloys and applied ns-PLAL to them to synthesize and disperse nanoparticles in water. Notably, in the case of the $Zr_{70}Cu_{15}Al_{10}Fe_5$ alloy, the ns-PLAL process resulted in the formation of amorphous nanowires. The possible formation mechanisms are spinnablity for nanowires and RP instability for nanoparticles, which are secondary to RT instability. To the best of our knowledge, this paper is the first report that addresses the key concept of "spinnability" to understand the formation mechanism of amorphous nanowires and to propose its importance in PLAL.

Optimization of optical laser parameters and chemical (material and environmental) conditions is expected to further improve selective wire formation, diameter and its distribution reduction, and stable dispersion.

Acknowledgments

The authors are grateful to H. Minamisawa and A. Kikuchi for their technical assistance at the Advanced Research Infrastructure for Materials and Nanotechnology in Japan (ARIM), Shinshu University. YM would like to thank JKA, Japan for the research support. This work was supported by JSPS KAKENHI Grant Number JP20K05278 and TAKEUCHI Scholarship Foundation's Research Grant.

References

[1] M. Haruta, T. Kobayashi, H. Sano, and N. Yamada: Chem. Lett., 16, (1987) 405.
[2] S. Iijima: Nature, 354, (1991) 56.
[3] T. Nagao, J. T. Sadowski, M. Saito, S. Yaginuma, Y. Fujikawa, T. Kogure, T. Ohno, Y. Hasegawa, S. Hasegawa, and T. Sakurai: Phys. Rev. Lett., 93, (2004) 105501.
[4] F. Li, Z. Zhang, H. Liu, W. Zhu, T. Wang, M. Park, J. Zhang, N. Bönninghoff, X. Feng, H. Zhang, J. Luan, J. Wang, X. Liu, T. Chang, J. P. Chu, Y. Lu, Y. Liu, P. Guan, and Y. Yang: Nat. Mater., 23, (2023) 52.
[5] G. Kumar, H. X. Tang, and J. Schroers: Nature, 457, (2009) 868.
[6] S.-X. Liang, L.-C. Zhang, S. Reichenbergera, and S. Barcikowski: Phys. Chem. Chem. Phys., 23, (2021) 11121.
[7] S. Ahadian, R. B. Sadeghian, S. Yaginuma, J. Ramón-Azcón, Y. Nashimoto, X. Liang, H. Bae, K. Nakajima, H. Shiku, T. Matsue, K. S. Nakayama, and A. Khademhosseini: Biomater. Sci., 3, (2015) 1449.
[8] Y. Liu, J. Liu, S. Sohn, Y. Li, J. J. Cha, and J. Schroers: Nat. Commun., 6, (2015) 7043.
[9] K. S. Nakayama, Y. Yokoyama, T. Wada, N. Chen, and A. Inoue: Nano Lett., 12, (2012) 2404.
[10] S. Yaginuma, C. Nakajima, N. Kaneko, Y. Yokoyama, and K. S. Nakayama: Sci. Rep., 5, (2015) 10711, and references therein.
[11] F. Mafuné, J. Kohno, Y. Takeda, and T. Kondow, and H. Sawabe: J. Phys. Chem. B, 104, (2000) 9111.
[12] V. Amendola, D. Amans, Y. Ishikawa, N. Koshizaki, S. Scirè, G. Compagnini, S. Reichenberger, and S. Barcikowski: Chem. – Eur. J., 26, (2020) 9206.
[13] C.-Y. Shih, M. V. Shugaev, C. Wu, L. V. Zhigilei, J. Phys. Chem. C, 121, (2017) 16549.
[14] X. Song, K. L. Xiao, X. Q. Wu, G. Wilde, and M. Q. Jiang: J. Non-Cryst. Solids, 517, (2019) 119.

[15] J. Eggers and E. Villermaux: Rep. Prog. Phys., 71, (2008), 036601.
[16] D. V. Louzguine-Luzgin, E. N. Zanaeva, F. R. Pratama, T. Wada, S. Ito: Scripta Mater., 231, (2023) 115468.
[17] Q. S. Zhang, W. Zhang, G. Q. Xie, D. V. Louzguine-Luzgin, A. Inoue: Acta Mater., 58, (2010) 904.
[18] R. Ninomiya, D. Kim; N. Takata, S. M. Lyth, K. Ishikawa, Y. Miyajima: Appl. Phys. Lett., 124, (2024) 201903.
[19] Y. Miyajima, H. Minowa, D. Tanada, P. P. Bhattacharjee, S. M. Lyth, K. Ishikawa: Opt. Laser Technol., 191, (2025) 113381.
[20] F. Ye and K. P. Musselman: APL Mater., 12, (2024) 050602.
[21] T. Tsuji, N. Watanabe, and M. Tsuji: Appl. Surf. Sci., 211, (2003) 189.
[22] R. G. Nikov, A. S. Nikolov, N. N. Nedyalkov, P. A. Atanasov, M. T. Alexandrov, and D. B. Karashanova: Appl. Surf. Sci., 274, (2013) 105.
[23] Y. Shimotsuma, T. Yuasa, H. Homma, M. Sakakura, A. Nakao, K. Miura, K. Hirao, M. Kawasaki, J. Qiu, and P. G. Kazansky: Chem. Mater., 19, (2007) 1206.
[24] C.-Y. Shih, R. Streubel, J. Heberle, A. Letzel, M. V. Shugaev, C. Wu, M. Schmidt, B. Gökce, S. Barcikowski, L. V. Zhigilei: Nanoscale, 10, (2018), 6900.
[25] C. A. Angel: Science, 267, (1995) 1924.
[26] K. Venkatakrishnan, D. Vipparty, and B. Tan: Opt. Express, 19, (2011) 15770.

(Received: June 30, 2025, Accepted: August 29, 2025)